Journal of the Korean Geographical Society, Vol.39, No.5, 2004(786~803)

Updating Land Cover Classification Using Integration of Multi-Spectral and Temporal Remotely Sensed Data

Dong-Ho Jang* and Chang-Jo F. Chung**

다중분광 및 다중시기 영상자료 통합을 통한 토지피복분류 갱신

장동호* · Chang-Jo F. Chung**

Abstract : These days, interests on land cover classification using not only multi-sensor data but also thematic GIS information, are increasing. Often, although we have useful GIS information for the classification, the traditional classification method like maximum likelihood estimation technique (MLE) does not allow us to use the information due to the fact that the MLE and the existing computer programs cannot handle GIS data properly. We proposed a new method for updating the image classification using multi-spectral and multi-temporal images. In this study, we have simultaneously extended the MLE to accommodate both multi-spectral images data and land cover data for land cover classification. In addition to the extended MLE method, we also have extended the empirical likelihood ratio estimation technique (LRE), which is one of non-parametric techniques, to handle simultaneously both multi-spectral images data and land cover data. The proposed procedures were evaluated using land cover map based on Landsat ETM+ images in the Anmyeon-do area in South Korea. As a result, the proposed methods showed considerable improvements in classification accuracy when compared with other single-spectral data. Improved classification images showed that the overall accuracy indicated an improvement in classification accuracy of 6.2% when using MLE, and 9.2% for the LRE, respectively. The case study also showed that the proposed methods enable the extraction of the area with land cover change. In conclusion, land cover classification produced through the combination of various GIS spatial data and multi-spectral images will be useful to involve complementary data to make more accurate decisions.

Key Words : land cover classification, GIS, maximum likelihood estimation, likelihood ratio estimation, data combination, classification accuracy

요약 : 최근, 다중 센서 영상과 GIS 주제도 정보를 이용한 토지 피복 분류에 대해 관심이 증가하고 있는 추세이다. 그러나, 분류에 필요한 효과적인 GIS 정보를 충분히 보유하고 있음에도 불구하고, 최대우도법(MLE) 같은 전통적인 방법은 기존의 컴퓨터 프로그램들이 GIS 자료를 제대로 다룰 수 없다는 이유로 유용한 정보의 이용에 제한을 받아 왔다. 본 연구에서는 다중 파장대 및 다중 시기 영상을 이용하여 새로운 영상 분류기법을 제안하고자 한다. 특히 MLE기법을 확대하여 다중 스펙트럼 영상 자료 및 토지 피복 분류 자료 등을 함께 사용할 수 있도록 하였다. 또한 파라미터가 데이터에서 추정되는 경우 우도비(LRE) 추정법이 오히려 더 적합할 수 있어서 LRE기법도 함께 사용하였다. 연구 지역은 서해안 안면도 지역이며, 자료는 Landsat ETM+ 영상과 Landsat TM 영상을 이용하여 만든 토지 피복도이다. 연구 결과, 제안된 방법은 단일 스펙트럼 자료를 사용하는 것보다 현저히 개선된 분류 정확도를 나타낸다. 즉, 개선된 분류 영상들은, MLE를 사용했을 때는 6.2%, LRE를 사용했을 때는 9.2%의 분류 정확도 개선을 보였다. 또한 본 연구는 제시된 알고리즘이 토지 피복 변화에 따른 그 지역의 변화 지역 추출도 가능할 것으로 판단된다. 향후 토지피복 분류 결과는 실 세계에서 보다 정확한 의사결정을 위한 보완적인 자료로써 유용하게 사용될 수 있을 것이라는 판단된다.

주요어 : 토지피복분류, 지리정보시스템, 최대우도법, 우도비, 자료통합, 분류정확도

* Instructor, National Research Laboratory (Harmful Algal Blooming Control), Kongju National University, gisrs@kongju.ac.kr

** Research Scientist, Geological Survey of Canada, chung@gsc.nrcan.gc.ca

1. Introduction

The studies on the interpretation of land covers require much detail for the understanding of the underlying processes. However, it is difficult to get accurate data about land cover features due to both the necessary manual activity and statistical analysis of large data sets. Nevertheless, it becomes a common knowledge that land cover classification can be greatly facilitated by the use of remotely sensed data owing to their wide area coverage, synchronism, periodicity and economical efficiency. Therefore, there are many advantages in using GIS and remotely sensed images for spatial data processing, the production of land cover map and modeling.

To perform the image classification, the combination of data from both multi-spectral images and multi-sensor images or other GIS classifications, can be utilized to reduce the classification error obtained by a multi-spectral classification. Conventional parametric classification methods require that the multi-spectral data be described by a common spectral density model. Such models cannot be easily established for combining different data types, e.g., spectral data from remotely sensed image and categorical data from a GIS. Another problem with the conventional approach is that different date sources might not be equally reliable. The development of an appropriate model for the classification of data from multi-sources and different numeric mode (e.g., a mixture of continuous and categorical data) is essential for more accurate land cover classification.

Recently, combination analyses using multi-spectral images, SAR data, GIS data have been made possible due to the development of data acquisition technology. It has led to the active progress of the study on land cover map making. Moreover, the combination between remote sensing information processing and GIS recently became universal. Thus, the combination analyses of satellite image information and GIS thematic map information have become important subjects. The proper combination analyses, using a combination of satellite image information and GIS thematic maps, would provide better quantitative results than those produced from the analysis of only one of two pieces of information. There are few studies however, in direct combination analyses of GIS spatial data and satellite data, which are directly related to these studies.

For multi-spectral data combination and classification within remote sensing applications, the important approaches include statistical methods(Lee *et al.*, 1987; Maselli, 1995; Solberg *et al.*, 1994; Solberg *et al*, 1996; Solberg, 1999; Tso and Mather, 1999; Warrender and Augusteijn, 1999), the neural networks(Benediktsson *et al*, 1997; Dai and Khorram, 1999; Guan *et al.*, 1997; Serpico *et al.*, 1996), fuzzy sets(Binaghi *et al*, 1997; Solaiman *et al.*, 1999), and evidence theory(Franklin *et al*, 2002; Peddle, 1995; Peddle and Ferguson, 2002). These studies included land cover classification: the development of new land cover classification techniques through the combination of multi-sensor/source remotely sensed images, and the accuracy verification of these techniques.

Several methodologies have been proposed to combine multi-source data for image classification improvement. Lee *et al.* (1987) focused on statistical methods for integrating different data sources, by extending the concepts used in Bayesian classification of multi-spectral images from one data source. The a posteriori probabilities are calculated for each data source independently, and the results are combined using a Bayesian combination rule. Solberg *et al* (1994) further extended this approach to accommodate data taken at different times, adding a term to account for the likelihood that the actual classification changed between the acquisition of the different data sets. Maselli *et al* (1995) proposed to integrate the information of ancillary data layers (morphology, pedology, etc.) into the classification process. The statistical basis of this probabilistic approach is described along with a procedure for the preliminary estimation of the information content expressed

by the ancillary data about the cover categories.

In another combined classification technique, Solberg *et al* (1996) suggested to a general model for multi-source classification of remotely sensed data based on Markov Random Field (MRF), and Solberg (1999) improved on Markov random field model for multi-source classification for forest map revision applications. Guan *et al.* (1997) applied contextual information using neural networks with which they built a quadratic regularizer. Binaghi *et al* (1997) presented a knowledge-based framework for contextual classification based on fuzzy set theory.

Peddle (1995) suggested multi-source evidential reasoning classification software system (MERCURYρ) based on the Dempster-Shafer theory of evidence. Franklin *et al* (2002) compared a multi-source Evidential Reasoning(ER) classification algorithm, capable of handling this large and diverse data set, to a more conventional maximum likelihood decision rule which could only use a subset of the available data. Research on combination of classification techniques is still at an early stage and much more exploration needs to be done.

To prepare land cover maps, supervised classification techniques have been widely used as effective tools to produce various thematic maps from satellite image data (Maxwell, 1976). Using the maximum likelihood estimation technique (MLE), especially, remotely sensed images have been recognized as an effective input to land cover classification. Recently, as fields of such application have broadened, interests on classification analysis using not only multi-sources images but also thematic GIS information have also grown. Often, although we have useful GIS information for the classification, the traditional MLE does not allow us to use the information, not because the data is not desirable but owing to the fact that the MLE and the existing computer programs cannot handle GIS data.

In this study, we have extended the MLE to accommodate both remotely sensed images and GIS data for land cover classification. MLE is based on the assumption that the distribution function of remotely sensed images of each land cover class is normal distribution with known parameters, the mean vector and the variance-covariance matrix (Press, 1972). However, in practice, although the normality assumption of the distribution functions is reasonable, it is not possible to assume that we know the mean vectors and the variance-covariance matrices of the distribution functions. In reality, these parameters are estimated from the input database. When the parameters are estimated from the data, theoretically MLE is not a right procedure (Press, 1972; McLallen, 1990) and the proper procedure is likelihood ratio estimation technique (LRE). We also have extended LRE to handle both remotely sensed images and GIS categorical data. We proposed to update land cover map by combining data from multi-sensor and multi-temporal satellite images. In other words, this study will be focused on updating land cover map through the combinations of Landsat TM and Landsat ETM+ data in multi-sensor and multi-temporal satellite data. The performance of the proposed model is investigated with combination of remotely sensed images and GIS spatial data for land cover classification. Accordingly, we attempted to make a land cover maps using Landsat TM data acquired in 1996, and then a new one by combining the classified land cover map into the Landsat ETM+ image, which was acquired in 1999, using the GIS spatial data.

The accuracy of this classification integration technique was verified by comparisons made with actual-measured validation data. The proposed procedure was evaluated using Landsat ETM+ images and existing land cover maps in the Anmyeon-do in Korea.

2. Methodologies

Parametric classification methods estimate the probability density functions of the classes from the

training data, under the assumption that they are distributed in a multivariate normal manner. In the MLE technique the sample class means and covariance matrices are considered valid estimates of the mean and covariance matrices of the classes. For supervised classification, we have employed both the Bayesian data combination method based on MLE and LRE techniques. In this study, we will briefly review the basic concepts of combination the estimates from categorized and continuous data layers and decision rule.

1) Basic Idea

Consider r land cover types to be constructed using a classification method in a study area. We will use k layers of categorized data layers and h layers of remotely sensed image data layers for the classification. We also assume that we have sufficient training data which is available for each land cover type in the study area. For a pixel p, let $(x_1, \cdots, x_k, y_1, \cdots, y_h)$ denote pixels values at p where the first k values, $x_1, \cdots, x_k$ correspond to the categorical data layers and subsequent h values, $y_1, \cdots, y_h$ represent the continuous data layers.

$$P\{\mathbf{M}_i \mid x_1, \cdots, x_k, y_1, \cdots, y_h\}, (i = 1, \cdots, r) \quad (1)$$

As usual, let denote the conditional probability that the pixel p belongs to the i^{th} class, $\mathbf{M}_i$ given that $(x_1, \cdots, x_k, y_1, \cdots, y_h)$ are pixels values at p. Often, the probability in (1) is also called "posterior" probability meaning that it is the probability that p belongs to $\mathbf{M}_i$ after observing k+h pixel values, $(x_1, \cdots, x_k, y_1, \cdots, y_h)$ at p.

If we know how to compute $P\{\mathbf{M}_i \mid x_1, \cdots, x_k, y_1, \cdots, y_h\}$ for every class i (i=1, ⋯, r) for a given pixel p with $(x_1, \cdots, x_k, y_1, \cdots, y_h)$, then the classification problem becomes very simple, in that, we assign the pixel p to the class g, if $P\{\mathbf{M}_g \mid x_1, \cdots, x_k, y_1, \cdots, y_h\}$ is the largest among all $P\{Mi \mid x1,, xk, y1,, yh\}$ (i=1,, r).

Using Bayes' theorem (Richards, 1995), we express the probability in (1) in the following form:

$$P\{\mathbf{M}_i \mid x_1, \cdots, x_k, y_1, \cdots, y_h\} = \frac{P\{x_1, \cdots, x_k, y_1, \cdots, y_h \mid \mathbf{M}_i\} P\{\mathbf{M}_i\}}{P\{x_1, \cdots, x_k, y_1, \cdots, y_h\}}, \quad (2)$$

where $P\{\mathbf{M}_i\}$ is the "prior" probability that the pixel p belongs to the i^{th} class, $\mathbf{M}_i$ before observing $(x_1, \cdots, x_k, y_1, \cdots, y_h)$ at p and it contrasts to the posterior probability in (1) and

$$P\{x_1, \cdots, x_k, y_1, \cdots, y_h\} = \sum_{i=1}^{r} P\{x_1, \cdots, x_k, y_1, \cdots, y_h \mid \mathbf{M}_i\} P\{\mathbf{M}_i\}. \quad (3)$$

There are several ways to estimate $P\{\mathbf{M}_i \mid x_1, \cdots, x_k, y_1, \cdots, y_h\}$, (i = 1, ⋯, r) from the training data. Instead of estimating $P\{\mathbf{M}_i \mid x_1, \cdots, x_k, y_1, \cdots, y_h\}$ directly in (1), we could try to obtain it by estimating, equivalently, $P\{x_1, \cdots, x_k, y_1, \cdots, y_h \mid \mathbf{M}_i\}$ and $P\{\mathbf{M}_i\}$ from the training data by using (2). Consider $P\{x_1, \cdots, x_k, y_1, \cdots, y_h \mid \mathbf{M}_i\}$, the conditional probability that the pixel p has $(x_1, \cdots, x_k, y_1, \cdots, y_h)$ observations, assuming that the pixel p comes from the i^{th} class, $\mathbf{M}_i$. In other words, it is the k+h multivariate frequency distribution function of the pixel values in the $\mathbf{M}_i$. Therefore, to estimate the posterior probability in (1) is equivalent to estimating the frequency distribution functions of the pixel values in r classes using the training data. The frequency distribution function of the class, $\mathbf{M}_i$ is usually expressed as $f\{x_1, \cdots, x_k, y_1, \cdots, y_h \mid \mathbf{M}_i\}$ instead of $P\{x_1, \cdots, x_k, y_1, \cdots, y_h \mid \mathbf{M}_i\}$.

2) Separation of Categorized Data Layers and Continuous Data Layers

To handle the multivariate frequency distribution functions of two different types of data layers, we have made the following assumption of conditional independence:

$$f\{x_1, \cdots, x_k, y_1, \cdots, y_h \mid \mathbf{M}_i\} = f\{x_1, \cdots, x_k \mid \mathbf{M}_i\} f\{y_1, \cdots, y_h \mid \mathbf{M}_i\}, (i = 1, \cdots, r). \quad (4)$$

Under the assumption of (4), the k + h dimensional multivariate frequency distribution function, $f\{x_1, \cdots, x_k, y_1, \cdots, y_h \mid \mathbf{M}_i\}$ is expressed as a multiple of the k dimensional multivariate discrete distribution function for the categorical data and the h dimen-

sional multivariate continuous distribution function for the continuous data and hence we will estimate the frequency distribution function as a multiple of two distribution functions, one for categorical data layers and the other for continuous data layers.

Under most practical circumstances, the conditional independent assumption in (4) is reasonable except for some of the categorized data layers were directly deducted from the continuous data layers

3) Estimation of Frequency Distribution Function for Categorized Data Layers

Among r frequency distribution functions, consider one $f\{x_1, \cdots, x_k \mid \mathbf{M}_i\}$ for a pixel p with k pixel values $(x_1, \cdots, x_k)$, each x_j representing a category in the j^{th} data layer where the pixel p belongs to $\mathbf{M}_i$ class. $f\{x_1, \cdots, x_k \mid \mathbf{M}_i\}$ is the $m_1 \times m_2 \times \cdots \times m_k$ cross-classified contingency table, where m_j represents the number of categories in the j^{th} layer. The $x_1 x x_2 x \cdots x x_k$ cell of the k-dimensional table represents the number of $\mathbf{M}_i$ class pixels that belongs to x_1 category in the 1^{st} layer, x_2 category in the 2^{nd} layer and x_k category in the k^{th} layer. Let us denote $U_{x_1 \cdots x_k}$ as the unique condition sub-area (Chung *et al.*, 1995; Clerici *et al.*, 2002) with the classes, $x_1, \cdots, x_k$ and the pixels in the sub-area belong to the x_1 category in the 1^{st} layer, the x_2 category in the 2^{nd} layer and the x_k category in the k^{th} layer. # of $\mathbf{M}_i$ class pixels within $U_{x_1 \cdots x_k}$ is the $x_1 x x_2 x \cdots x x_k$ cell of the k-dimensional table.

The first non-parametric estimate of $f\{x_1, \cdots, x_k \mid \mathbf{M}_i\}$ is the empirical frequency distribution function from the training data:

$$\breve{f}\{x_1, \cdots, x_k \mid \mathbf{M}_i\} = \#\text{ of } \mathbf{M}_i \text{ class pixels within } U_{x_1 \cdots x_k} \text{ from the training data.} \quad (5)$$

However, if we assume that $f\{x_1, \cdots, x_k \mid \mathbf{M}_i\}$ is the multivariate multinomial frequency distribution functions (Johnson and Kotz, 1972). Then, the maximum likelihood estimate of this multinomial distribution function is the empirical k-dimensional contingency table in (5). Although it is simple to compute, but we strongly suggest NOT using the estimate in (5), when the number of categorized data layers is more than two.

The second procedure to estimate $f\{x_1, \cdots, x_k \mid \mathbf{M}_i\}$, $(i = 1, \cdots, r)$ assumes, as in (4), that the k categorical layers are conditionally independent and hence, we have:

$$f\{x_1, \cdots, x_k \mid \mathbf{M}_i\} = f\{x_1 \mid \mathbf{M}_i\} \cdots f\{x_k \mid \mathbf{M}_i\}, (i = 1, \cdots, r). \quad (6)$$

Instead of considering all the k layers at the same time, we may estimate the distribution function as a multiple of k separate distribution functions. Each separate function is estimated by the empirical frequency distribution function using each single categorical data layer:

$$\tilde{f}\{x_j \mid \mathbf{M}_i\} = \#\text{ of } \mathbf{M}_i \text{ class pixels within } x_j \textit{ category} \text{ within the } j^{th} \text{ layer} \quad (7)$$

Using (6) and (7) under the conditional independence assumption, we obtain an empirical estimate of $f\{x_1, \cdots, x_k \mid \mathbf{M}_i\}$ by:

$$\tilde{f}\{x_1, \cdots, x_k \mid \mathbf{M}_i\} = \tilde{f}\{x_1 \mid \mathbf{M}_i\} \cdots \tilde{f}\{x_k \mid \mathbf{M}_i\}, (i = 1, \cdots, r). \quad (8)$$

As before, if we assume that $f\{x_1, \cdots, x_k \mid \mathbf{M}_i\}$ is the multivariate multinomial frequency distribution functions and the conditional independence in (6), then, the empirical frequency function in (8) is also the maximum likelihood estimate of $f\{x_1, \cdots, x_k \mid \mathbf{M}_i\}$. We strongly recommend the use of equation (8) rather than (5), when the number of categorized data layers is more than two. When the number is greater than two and the number of the classes in each layer, is more than five, then the sizes of many of the unique condition sub-areas become very small and consequently many of the $\breve{f}\{x_1, \cdots, x_k \mid \mathbf{M}_i\}$ are equal to zero. When we integrate the zero value with the estimate of the frequency distribution function from the continuous data layers, they generate an undesirable negative impact on the prediction maps.

4) Estimation of Frequency Distribution Function for Continuous Data Layers

Consider the frequency distribution function for

continuous data layers, $f\{y_1, \cdots, y_k \mid \mathbf{M}_i\}$ for a pixel p with h pixel values $(y_1, \cdots, y_k)$, where each y_j represents a real value at y within the j^{th} continuous data layer. The simplest non-parametric estimate for the function is an empirical frequency distribution function based on either histogram or kernel method (reference). When the number of layers is more than two, then such empirical distribution is not recommended as an estimate. The next non-parametric procedure requires conditional independence as in (4). We assume that the h continuous layers are conditionally independent and hence, we have:

$$f\{y_1, \cdots, y_k \mid \mathbf{M}_i\} = f\{y_1 \mid \mathbf{M}_i\} \cdots f\{y_k \mid \mathbf{M}_i\}, (i = 1, \cdots, r). \quad (9)$$

Instead of considering k-dimensional multivariate distribution functions, we may estimate the frequency distribution function as a multiple of k separate univariate frequency distribution functions, where each univeriate individual distribution is estimated by an empirical frequency distribution:

$$\ddot{f}\{y_1, \cdots, y_k \mid \mathbf{M}_i\} = \ddot{f}\{y_1 \mid \mathbf{M}_i\} \cdots \ddot{f}\{y_k \mid \mathbf{M}_i\}, (i = 1, \cdots, r). \quad (10)$$

In many situations, the estimate in (7) is an effective estimate of $f\{y_1, \cdots, y_h \mid \mathbf{M}_i\}$. A parametric estimate of $f\{y_1, \cdots, y_h \mid \mathbf{M}_i\}$ is obtained by assuming that it is the multivariate normal distribution functions, $N(\mu_{\mathbf{M}_i}, \Sigma_{\mathbf{M}_i})$ where $\mu_{\mathbf{M}_i}$ are $\Sigma_{\mathbf{M}_i}$ the k-dimensional mean vectors for $\mathbf{M}_i$ class and the k x k dimensional covariance matrix for $\mathbf{M}_i$, respectively. Suppose that $\hat{\mu}_{\mathbf{M}_i}$ are $\hat{\Sigma}_{\mathbf{M}_i}$ the sample mean vector and the sample covariance matrix computed from the training data, then they are the maximum likelihood estimates of $\mu_{\mathbf{M}_i}$ and $\Sigma_{\mathbf{M}_i}$ (Hubert-Moy *et al.*, 2001). Using these MLE (Richards, 1995) we obtain the following estimate:

$$\ddot{f}\{y_1, \cdots, y_h \mid \mathbf{M}_i\} = \frac{1}{\sqrt{2\pi \left|\hat{\Sigma}_{\mathbf{M}_i}\right|}} \exp\left\{-\frac{1}{2}(y - \hat{\mu}_{\mathbf{M}_i})' \hat{\Sigma}_{\mathbf{M}_i}^{-1} (y - \hat{\mu}_{\mathbf{M}_i})\right\}, \quad (11)$$

where $y = (y_1, \cdots, y_h)$ is an h-dimensional vector containing h observed values and the computation operations in (11) are vector and matrix calculations.

However, as discussed in Press (1972), instead of the normal distribution with the sample mean vector and the sample covariance matrix in (11), the proper distribution function under the normal assumption with the sample mean vector and covariance matrix is the multivariate Student t-distribution function:

$$\tilde{f}\{y_1, \cdots, y_k \mid \mathbf{M}_i\} = \frac{\left[\frac{N_i}{(N_i + 1)\pi}\right]^{h/2} \frac{\Gamma\left(\frac{N_i}{2}\right)\hat{P}i}{\Gamma\left(\frac{N_i - h}{2}\right)\left|(N_i - 1)\hat{\Sigma}_{\mathbf{M}_i}\right|^{1/2}}}{\left[1 + \frac{N_i}{(N_i^2 - 1)}(y - \hat{\mu}_{\mathbf{M}_i})' \hat{\Sigma}_{\mathbf{M}_i}^{-1} (y - \hat{\mu}_{\mathbf{M}_i})\right]^{N_i/2}}, \quad (12)$$

where $\hat{P}i$ is an estimate of the prior probability, $P\{\mathbf{M}_i\}$. It should be used as an estimate of $f\{y_1, \cdots, y_h \mid \mathbf{M}_i\}$ instead of one in (11).

If the normality assumptions are reasonably realistic conditions, then we recommend the estimate shown in (12), but the estimate is almost similar to that in (11) of the maximum likelihood estimate. In practice, most of commercial computer packages don't have a computer program for (12). In this case, we recommend the use of (11) instead of (12) because the values are almost identical. However, if the empirical distribution functions appear to be far from the normality, then we recommend the estimate in (10) under the conditional independence assumption.

5) Combining the Estimates from Categorized and Continuous Data Layers and Decision Rule

Under the assumption of (13), the k + h dimensional multivariate frequency distribution function, $f\{x_1, \cdots, x_k, y_1, \cdots, y_h \mid \mathbf{M}_i\}$ containing both the categorized and continuous data layers can be expressed as a multiple of the discrete distribution function for the categorical data and the continuous distribution function for the continuous data and we have discussed how these estimates could be obtained from the training data. We obtained an estimate of $f\{x_1, \cdots,$

$x_k, y_1, \cdots, y_h \mid \mathbf{M}_i\}$ by:

$$\hat{f}\{x_1, \cdots, x_k, y_1, \cdots, y_h \mid \mathbf{M}_i\} = \hat{f}\{x_1, \cdots, x_k \mid \mathbf{M}_i\}\ \hat{f}\{y_1, \cdots, y_h \mid \mathbf{M}_i\}, \quad (13)$$

where $\hat{f}\{x_1, \cdots, x_k \mid \mathbf{M}_i\}$ is obtained by either (5) or (8) and $\hat{f}\{y_1, \cdots, y_h \mid \mathbf{M}_i\}$ is obtained by one of (10), (11) and (12). For every pixel with k+h pixel values, $(x_1, \cdots, x_k, y_1, \cdots, y_h)$, we compute $\hat{f}\{x_1, \cdots, x_k, y_1, \cdots, y_h \mid \mathbf{M}_i\}$, one for each class, i = 1, ⋯, r. Then we assign the pixel p to the class g, if $\hat{f}\{x_1, \cdots, x_k, y_1, \cdots, y_h \mid \mathbf{M}_g\}$ is the largest among all $\hat{f}\{x_1, \cdots, x_k, y_1, \cdots, y_h \mid \mathbf{M}_i\}$ (i=1, ⋯, r).

3. Study Area and Data Collection

During the past decades, the western coastal area of Korea has experienced serious environmental changes due to reclamation work, and the construction of industrial complexes and similar infrastructures in the area. For this matter, it is well known that issues on the environmental or ecological damage are essential things that should be considered. To the end, we find it necessary to discover a new technique that can detect wide-ranging changes of land cover.

This study area covers approximately 128 km^2, located on the southern coast of the village of *Taean-gun* in the *Chungnam province*, of western Korea, as shown in Figure 1. It lies between 126°18′30″and 126°26′26″ East of longitude and 36°23′35″ and 36°36′50″ North of latitude. *Anmyeon-do* is a narrow elongated island that boasts a National Coastal Park that includes numerous beaches. In addition, a natural bay named *Cheonsu-bay* is located along the east coast and it makes a wide tidal flat during the ebb

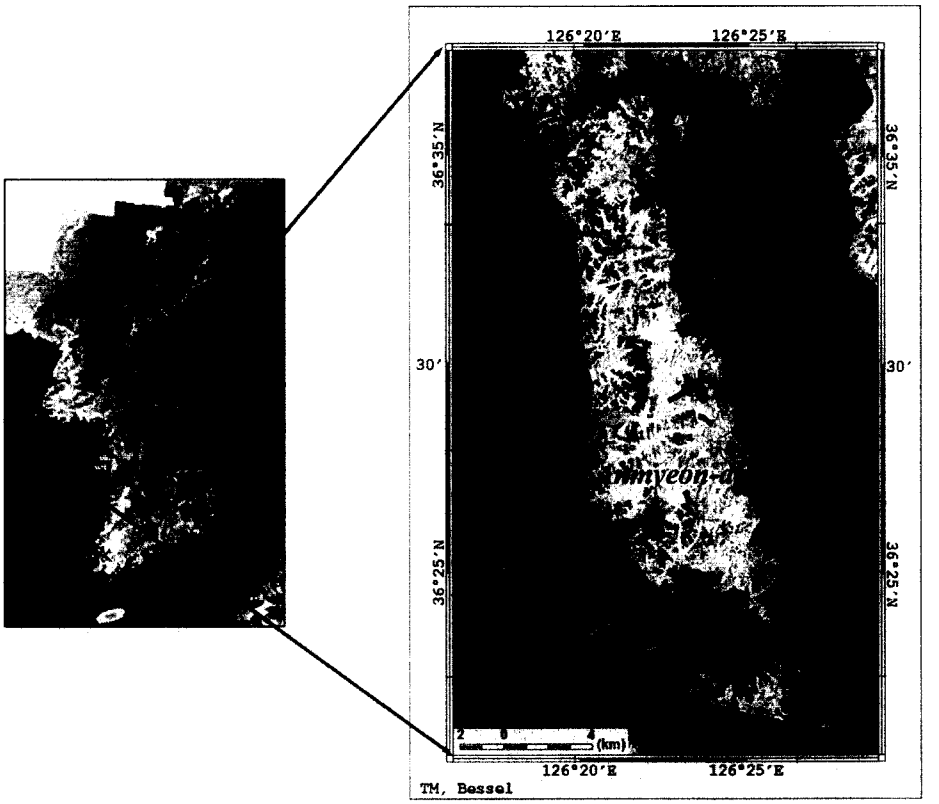

Figure 1. The location of the Taean-gun area in Korea (Landsat ETM+ image of 1999. 10.20)

tide. Recent reclamation schemes and tourist resort developments have triggered rapid changes in the costal environment.

The Landsat TM images and Landsat ETM+ images were acquired on 1 September 1996, and 20 October 1999, respectively. They are very complex scenes due to the great mixture of surface features and the spatial variability of the land cover. The images were registered to the Universal Transverse Mercator coordinate system using 1:25,000 topographic maps. In this study, the ocean water class showed a prominent discrepancy in reflection and it was masked using the digital topographic maps and band 4 of Landsat ETM+ imagery.

On the basis of an extensive knowledge of the area and an accurate ground survey carried out during the period of 1999-2000, nine classes were found to be representative of the land cover, as shown in Table 1. Defined nine classes in the study are as follows: "water" (lake), "tidal flat", "saltpan", "sand", "forest", "pasture", "bare land", "farmland" and "urban area".

The training data were extracted from the screen digitizing of digital maps, aerial photography, and ground survey. The same training data were used for comparing different classification techniques. In this study, we selected 7,763 and 15,174 of training data from Landsat TM and Landsat ETM+, respectively, then used them to compare the classification method and to analyze the GIS multi-source combination analysis.

Table 1. Numbers of training and validation pixels by the land-cover classes over the study area.

Class	1996		1999	
	Training pixels	Validation pixels	Training pixels	Validation pixels
water	632	31	1035	29
tidal flat	997	42	1087	42
saltpan	824	24	1211	23
sand	556	23	800	23
forest	2139	110	4210	110
pasture	544	61	1181	61
bare land	477	21	421	22
farmland	1060	152	4716	155
urban area	534	35	513	35
Total	7763	499	15174	500

We first classified Landsat TM (1996) and then the Landsat ETM+ (1999) data were classified to update land cover map generated by using the Landat TM (1996). We used both the MLE and LRE techniques as well as six bands excluding the thermal band. Before applying the LRE technique, the PCA was performed firstly to remove noises caused by compression from multi-spectral data. We analyzed the correlation of each band after performing the PCA for both Landsat TM and Landsat ETM+ images. Then we selected the first three elements that will be used in the correlation analysis with training data.

We updated the land cover map by combining each one made by the MLE and LRE techniques in Landsat TM data (1996) into the Landsat ETM+ data (1999). This study used both the MLE and LRE techniques, which is the same as the 1996 land cover classification techniques. We then computed the classification accuracy using reference data.

To compute classification accuracy, we constructed a classification error matrix. There was a tendency to overestimate overall if the training set area was used in the classification error matrix. Reference data that are independent of the training data were collected by field survey. We selected sites exhibiting uniform spectral characteristics that are evenly located in the study area. The number of reference pixels used for the supervised classification was 499 in Landsat TM and 500 in Landsat ETM+, respectively (Table 1).

4. The Result of Multi-sensor and Multi-temporal Classification

1) Principal Component Analysis

PCA is an analysis method, which can effectively

handle many multi or hyperspectral bands due to its ability to compress data. Therefore, the PCA can be used not only in the land cover classification but also in water quality analysis, vegetation collation, multi-temporal data analysis, image combination and more.

Table 2 showed the PCA result, which revealed that the sum of the variance value of PC1, PC2, and PC3 at TM and ETM was 99.77%, 99.34%, respectively. This meant that most of the land cover information is included in PC1, PC2, and PC3.

Fig. 2 showed the LRE function value of each principal component of Landsat TM, as calculated using LRE. Generally, the PC1 image is very similar to the infrared band image and it has information from six bands. As it includes much information from bands 4 and 5, it especially appears dark in water and forest areas. As shown from Fig. 2(a), density value is higher in "water", "saltpan", "forest", and "tidal flat" areas. These categories almost showed normal distribution. However, "bare land", "urban", "sand", and "pasture" areas showed mixed values in the LRE function, and these land areas showed similar values in the LRE function.

The PC2 image is usually the reversed image of PC1. It also has most information from band 4. As shown from Fig. 2(b), these categories generally showed similar values in "sand", "forest" and "tidal flat" areas. These display normal distribution in their categories. "Urban" and "bare land", "water" and "saltpan" areas of mixed categories showed similar values for a wide range.

The PC3 image an excessive compression of data; and it is effective in perceiving drainage network and urban area, because much information is acquired from band 5. Although "bare land" and "farmland" are distinguished in Fig. 2(c), other categories show similar values covering wide ranges like PC2. Although PC4, PC5, and PC6 have much information, these are not used in land cover classification due to the presence of noise and their excessive compression.

2) Result of Land Cover Map Using Landsat TM Data (1996)

In this study, we improved the land cover classification using multi-temporal image data. We conducted land cover classification by using Landsat TM data acquired in 1996.

According to the results of image classification, the classification accuracy of MLE and LRE shows a striking difference. As shown from Table 3, an overall accuracy at MLE and LRE is 83.80% and 77.60%, respectively and the difference of classification accuracy is 6.2%. In kappa statistic, the MLE and the LRE techniques were 0.80% and 0.73%, respectively. As to this classification error, MLE shows relatively higher classification accuracy, as most of the training data from Landsat TM data have normal distribution (Fig. 2). User's accuracy of MLE exhibited classification accuracy of over 80 % for most class categories. However, "bare land", "urban area" and "sand" showed lower classification accuracy than other class categories. MLE in "bare land" especially showed

Table 2. Eigenstructure of PCA results from Landsat TM and Landsat ETM+ data.

Eigenchannel	Landsat TM(1996. 9. 1)				Landsat ETM+(1999.10.20)			
	Eigenvalue	Deviation	%Variance	Σ%Variance	Eigenvalue	Deviation	%Variance	Σ%Variance
1	5699.6567	75.4961	93.40%	93.40%	2227.6570	47.1981	87.93%	87.93%
2	260.8518	16.1509	4.27%	97.67%	207.8450	14.4168	8.20%	96.13%
3	127.8654	11.3078	2.10%	99.77%	81.2052	9.0114	3.21%	99.34%
4	10.9714	3.3123	0.18%	99.95%	11.4768	3.3877	0.45%	99.79%
5	2.6764	1.6360	0.04%	99.99%	3.6834	1.9192	0.15%	99.94%
6	0.5680	0.7537	0.01%	100.0%	1.6237	1.2743	0.06%	100.0%

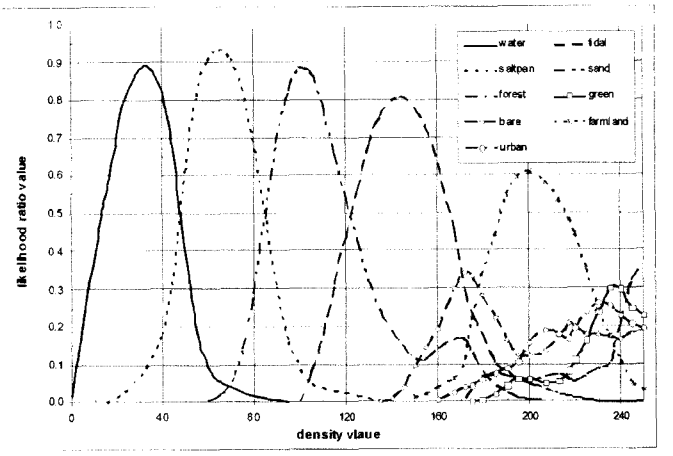

(a) PC1

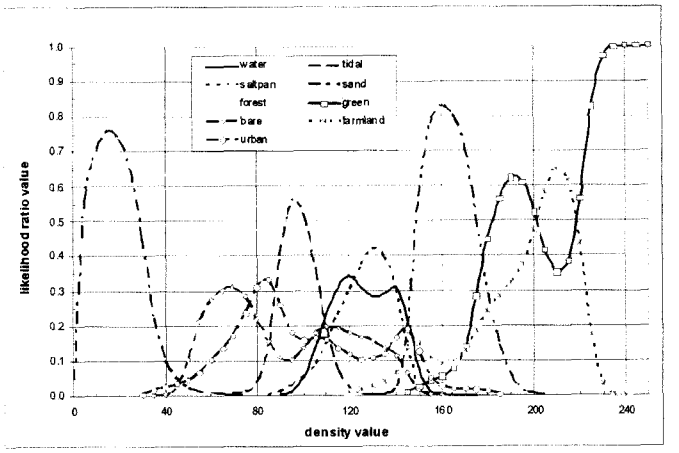

(b) PC2

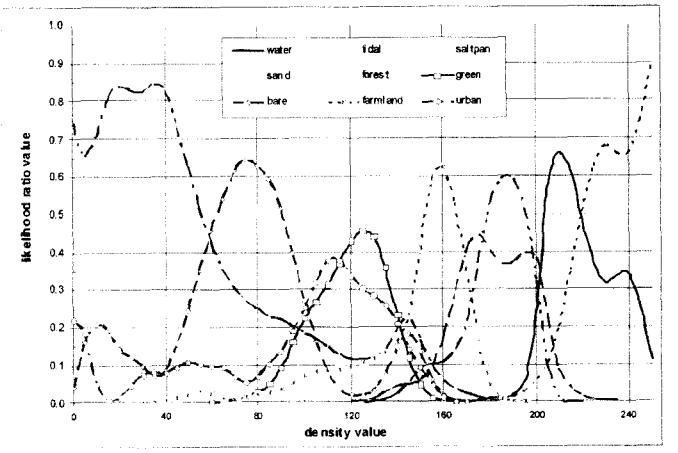

(b) PC3

Figure 2. Likelihood ratio functions for (a) PC1, (b) PC2, (c) PC3

Table 3. Calculated error matrices for the supervised classification using Landsat TM images (1996. 9. 1) (a) MLE (b) LRE

(a) maximum likelihood estimation		From validation									
		water	Tidal flat	saltpan	sand	forest	pasture	Bare land	Farm land	urban area	User's Accuracy(%)
From image classification	water	23	0	4	0	0	0	0	0	0	85.71
	tidal flat	0	42	0	4	1	0	1	0	0	87.50
	saltpan	3	0	19	0	0	0	0	1	0	82.61
	sand	0	0	0	19	1	0	4	1	1	73.08
	Forest	1	0	0	0	91	2	0	4	0	92.86
	pasture	0	0	0	0	0	47	0	4	0	92.16
	bare land	0	0	0	0	1	1	14	4	0	70.00
	farmland	3	0	1	0	14	9	0	133	4	81.10
	urban area	0	0	0	0	2	2	2	5	30	73.17
	Producer's Accuracy(%)	74.42	100.0	79.17	82.61	82.73	77.05	66.67	87.50	85.71	

Overall Accuracy = 83.80%, Overall Kappa Statistic = 0.803%

(b) likelihood ratio estimation		From validation									
		water	Tidal flat	saltpan	sand	forest	pasture	Bare land	Farm land	urban area	User's Accuracy(%)
From image classification	Water	24	0	7	0	0	0	0	0	0	77.42
	tidal flat	0	42	0	6	1	0	2	0	1	80.77
	saltpan	2	0	16	0	0	0	0	1	0	84.21
	sand	0	0	0	15	0	0	0	0	4	78.95
	forest	2	0	0	1	100	4	1	12	3	81.30
	pasture	0	0	0	0	1	49	0	25	1	64.47
	bare land	0	0	0	0	1	2	13	5	1	59.09
	farmland	3	0	1	0	6	6	2	108	4	83.08
	urban area	0	0	0	1	1	0	3	1	21	77.78
	Producer's Accuracy(%)	77.42	100.0	66.67	65.22	90.91	80.33	61.91	71.05	60.00	

Overall Accuracy =77.60%, Overall Kappa Statistic = 0.729%

70.00%, the lowest figures in classification accuracy. As to user's accuracy at LRE, "bare land" and "pasture" areas show the lowest classification accuracy, with 59.09% and 64.47%, respectively. This is caused by the similarity in spectral information in "bare land" and "pasture" of MLE and LRE because of the spectral recording in autumn, a seasonal factor.

As to producer's accuracy at MLE, "bare land", "pasture" and other similar categories show a relatively low classification accuracy like user's accuracy. The classification accuracy of class categories is 66.67 % and 77.05%, respectively. "Water" also shows a low classification accuracy, with its producer's accuracy at 77.42%. The low classification accuracy of "water" owes to its similarity in spectral information to that of "saltpan" and "farmland", as the density of suspend sediments and the chlorophyll-a of some lakes becomes higher. Most of other class categories have a producer's accuracy that is lower than 70% at LRE. Its value in "urban area" and "bare land" is 60.00% and 61.91%, respectively, showing the lowest classification accuracy.

Each land cover map acquired by the results above shows a low classification accuracy.

Nevertheless, it was used as the main GIS multi-source data used to update the land cover maps through the combining with the 1999 Landsat ETM+ data.

3) Updating Land Cover Maps Using Land Cover Map (1996)

This section concerns land cover classification using Landsat ETM+ images, and a land cover map updated through the combination of the land cover map that was acquired from the 1996 Landsat TM images and was integrated into the 1999 Landsat ETM+ images.

In the multi-spectral image classification of Landsat ETM+ data using MLE, an overall accuracy shows 81.40% while Kappa shows 0.78% (Table 4). These show a lower classification accuracy than the 1996 images classification. "Pasture" and "saltpan" at user's accuracy were 60.24% and 62.96%, showing the lowest classification accuracy. The low classification accuracy of "pasture" is due to the similarity of spectral information to "farmland" areas, as caused by a seasonal factor (autumn). In the case of "saltpan", it was due to spectral information being similar to "water" (caused

Table 4. Calculated error matrices for the MLE. (a) Landsat ETM+ data (b) Landsat ETM+ and Land cover map (Landsat TM)

(a) Landsat ETM+(1999)		From validation									
		water	Tidal flat	saltpan	sand	forest	pasture	Bare land	Farm land	urban area	User's Accuracy(%)
From image classification	water	21	0	1	0	0	0	0	0	0	95.46
	tidal flat	0	36	1	0	0	0	0	3	1	87.81
	saltpan	9	0	17	0	0	0	0	1	0	62.96
	sand	0	4	0	22	0	0	1	0	0	81.48
	forest	0	0	0	0	95	11	0	5	0	85.59
	pasture	0	0	0	0	11	50	0	22	0	60.24
	bare land	0	2	0	1	0	0	19	3	0	76.00
	farmland	3	0	0	1	2	0	1	117	4	91.41
	urban area	0	0	0	0	1	0	1	4	30	83.33
	Producer's Accuracy (%)	63.64	85.71	89.48	91.67	87.16	81.97	86.36	75.48	85.71	

Overall Accuracy = 81.40%, Overall Kappa Statistic = 0.776%

(b) Landsat ETM+ and Land-cover map(Landsat TM)		From validation									
		water	Tidal flat	saltpan	sand	forest	pasture	Bare land	Farm land	urban area	User's Accuracy(%)
From image classification	water	25	0	1	0	0	0	0	0	0	96.15
	tidal flat	0	37	0	0	0	0	0	3	0	92.50
	saltpan	5	0	18	0	0	0	0	0	0	78.26
	sand	0	4	0	22	0	0	1	0	1	78.57
	forest	0	0	0	0	98	5	0	2	0	93.33
	pasture	0	0	0	0	3	55	0	10	0	80.88
	bare land	0	1	0	1	0	0	20	5	0	74.07
	farmland	3	0	0	1	6	1	0	132	3	90.41
	urban area	0	0	0	0	2	0	1	3	31	83.78
	Producer's Accuracy (%)	75.75	88.10	94.74	91.67	89.91	90.16	90.91	85.16	88.57	

Overall Accuracy = 87.6%, Overall Kappa Statistic = 0.850%

by the presence of freshwater). "Water" and "farmland" show the lowest classification accuracy at producer's accuracy, and their values are 63.64% and 75.48%, respectively. The reason behind this result is the same as that of overall accuracy.

In the multi-spectral image classification of Landsat ETM+ data using LRE, an overall accuracy is 75.20% while Kappa is 0.70% (Table 5). This shows a lower classification accuracy than the 1996 images classification. "Bare land" and "pasture" at user's accuracy were at 44.83% and 54.80%, showing the lowest classification accuracy. The low classification accuracy of these class categories was caused by spectral information getting mixed with "farmland" areas (caused by the seasonal factor of autumn). "Urban" and "bare land" show the lowest classification accuracy at producer's accuracy, and its value is 57.14% and 59.09%, respectively. "Urban" areas have similar spectral information to that of "bare land" and "farmland" areas. Result from "bare land" was due to the mix of spectral information in "farmland" and "urban area". Updating land cover classification, in combination Landsat ETM+ and land cover map (using Landsat TM), showed a high-

Table 5. Calculated error matrices for the LRC. (a) Landsat ETM+ data. (b) Landsat ETM+ and Land-cover map (Landsat TM)

(a) Landsat ETM+		From validation									
		water	Tidal flat	saltpan	sand	forest	pasture	Bare land	Farm land	urban area	User's Accuracy(%)
From image classification	water	29	0	2	0	0	0	1	0	0	90.63
	tidal flat	0	40	1	2	0	0	1	4	1	81.63
	saltpan	0	0	15	0	0	0	0	0	0	100.00
	sand	0	1	0	18	0	0	0	0	1	90.00
	forest	2	0	0	1	100	10	0	10	0	81.30
	pasture	0	0	0	0	2	40	0	30	1	54. 80
	bare land	0	0	0	0	1	1	13	8	6	44.83
	farmland	2	0	1	0	6	10	4	101	6	77.69
	urban area	0	1	0	3	0	0	3	2	20	68.97
	Producer's Accuracy (%)	87.88	95.24	78.95	75.00	91.74	65.57	59.09	65.16	57.14	

Overall Accuracy = 75.20%, Overall Kappa Statistic = 0.700%

(b) Landsat ETM+ and Land-cover map(Landsat TM)		From validation									
		water	Tidal flat	saltpan	sand	forest	pasture	Bare land	Farm land	urban area	User's Accuracy(%)
From image classification	water	30	0	1	0	0	0	1	0	0	93.75
	tidal flat	0	40	1	0	0	0	1	3	1	86.96
	saltpan	0	0	16	1	0	0	0	1	0	88.89
	sand	0	1	0	18	0	0	0	0	0	94.74
	forest	0	0	0	1	99	5	1	6	0	88.40
	pasture	0	0	0	0	2	46	0	3	0	90.20
	bare land	0	0	0	1	1	1	14	9	0	53. 85
	farmland	3	0	1	0	7	8	2	130	5	83.33
	urban area	0	1	0	3	0	1	3	3	29	72.50
	Producer's Accuracy (%)	90.91	95.24	84.21	75.00	90.83	75.41	63.64	83.87	82.86	

Overall Accuracy = 84.4%, Overall Kappa Statistic = 0.810%

er classification accuracy than the land cover classification with single-spectral information. Table 4 and Table 5 listed Kappa statistics in MLE and LRE with 0.85% and 0.81%, respectively. The overall accuracy for MLE was 87.06% and one for LRE was 84.40%. That indicated an improvement of 6.2% in MLE and 9.2% in LRE. In these categories of user's accuracy, both showed a high classification accuracy of over 80% in most of their class categories. However, "bare land", "urban area", "saltpan", and "sand" classification accuracy had a lower accuracy in classification. "Bare land" in particular, presented an accuracy of LRE and MLE with 53.85% and 74.07%, respectively. This resulted from the classification of "bare land" in the land cover map of 1996 as the "farmland" in the site investigation, and from the single-spectral image classification.

At producer's accuracy, the classification of MLE and LRE shows a relatively striking difference. While the "water" class category shows 75.75% accuracy, which is the lowest value in the case of MLE, "water" shows the highest accuracy, which is 90.91% at LRE. On the other hand, "bare land" shows the lowest accuracy of 63.64% at LRE, but it gave the highest accuracy, 90.91% at MLE. The reason behind these contrary results is believed to be because MLE is the combination classification that is based on spectral information of Landsat images, while LRE shows different class categories in updating by using the PCA data. It is also believed that if we make the land cover maps by updating the results of these classification methods, we will have better results than we had in combination the classification method with the existing individual classification techniques.

According to the comparison made above between single-spectral image classifications and updating of image classifications, the updating land cover map exhibited better classification with a higher accuracy in all MLE and LRE techniques. This has been interpreted as a consequence of the proper representation of spatial image information of land cover map (using Landsat TM) data with the combination MLE and LRE techniques. The results of land cover classification can be seen in the study area where the user's accuracy for each class categories supports the improvement in classification accuracy; using GIS multi-source data in classification resulted in improved accuracy for every class categories (Table 4, Table 5). At user's accuracy, "pasture" areas especially show improved effects: 35.4% at LRE and 20.64% at MLE. Although single-spectral image classification shows similar spectral information as that of the other classification categories (owing to the seasonal factor), we attained an improved classification accuracy for "pasture" areas by classifying the combination of land cover maps that were made in other seasons.

The improvement of low classification accuracy was done through updating image classification. Figure 3 shows a decrease in land cover classification for "pasture" and "bare land" where both Landsat ETM+ and land cover map (Landsat TM) were used. Many areas classified as "pasture" in single-spectral image classification were updated as "farmland" by land cover map (Landsat TM). In producer's accuracy, the use of land cover map (Landsat TM) data improved the accuracy in classification for most class categories. Especially, the LRE technique producer's accuracy in "urban area" and "farmland" improved by 25.7% and 18.7%, respectively. We attained to improved classification accuracy for "pasture" areas, mainly because of the improvement of the "farmland" category. Figure 3 shows local changes of "pasture" into "urban area" or "farmland". This shows that accomplishing land cover classification using the existing GIS multi-source data could enable the extraction of the area with changes in land cover.

5. Discussion and Conclusions

Recently, as various fields of application have

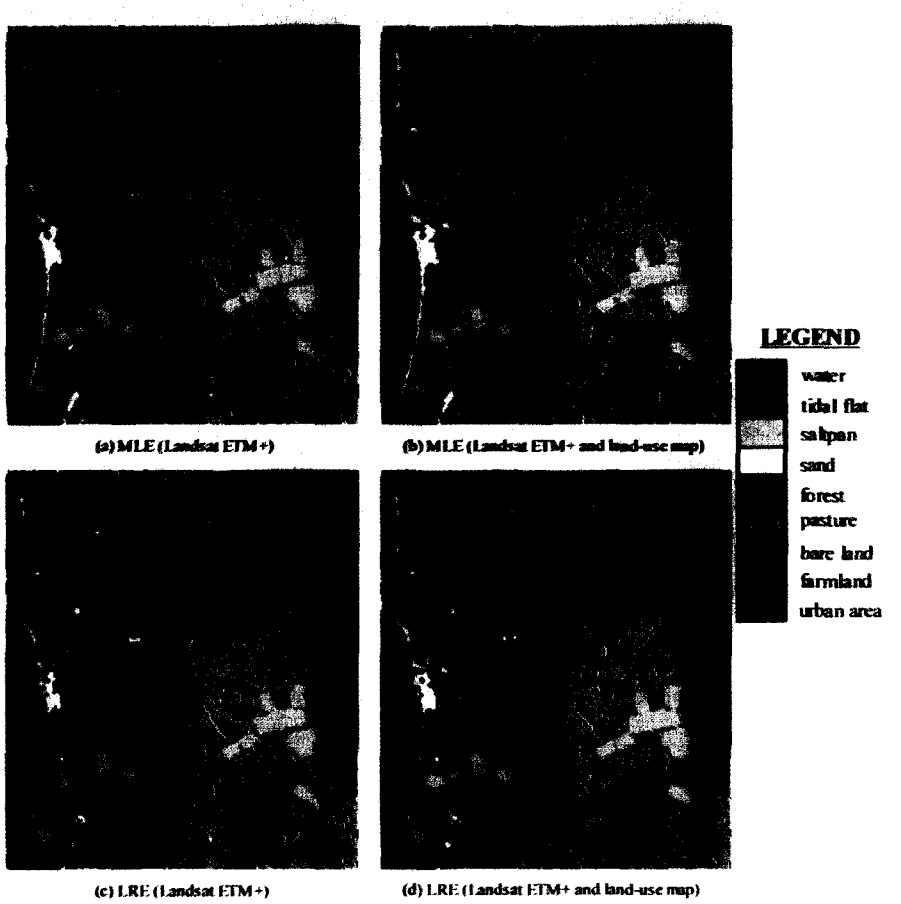

Figure 3. Land cover map of classification from MLE and LRE using Landsat ETM+ and land cover map (Landsat TM)

broadened, interests on classification analysis using not only multi-sources images but also thematic GIS information have also grown. Advantages of maximum likelihood estimation technique have led to a great extent spread of its use for remote sensing application. This has also encouraged research communities towards possible improvements and extensions of the basic procedure. However, even if we have useful GIS information for the classification, the traditional MLE does not allow us to use information, not because the data are not desirable but owing to the fact that the MLE and existing computer programs cannot handle GIS data properly. Moreover, although the normality assumption of the distribution functions is reasonable, it is not possible to assume that we know the mean vectors and the variance-covariance matrices of the distribution functions. These parameters are estimated from the input database. When the parameters are estimated from data, theoretically speaking, MLE is not the right procedure and the proper procedure is likelihood ratio estimation technique.

In this paper, we had extended the MLE and LRE to accommodate for land cover classification. In particular, the performance of the proposed updating classification techniques was investigated by combination remotely sensed images and GIS spatial data. The PCA was performed in order to calculate the LRE value in updating data using the LRE technique. We also incorporate a priori information about the

probability of changes between the acquisitions of the different data to be integrated. By updating spectral imageries with thematic GIS data, a more accurate interpretation of the scene can be obtained. The updating results from the proposed method showed considerable improvements in classification accuracy, as compared with other multi-spectral classification techniques. In particular, updating land cover classification, in updating Landsat ETM+ imageries and land cover map (Landsat TM), showed higher accuracy than the land cover classification with multi-spectral information.

The result of updating land cover classification using remotely sensed images with GIS thematic data appeared as an improvement in the overall accuracy of 6.2% in MLE and 9.2% in LRE classification, respectively. This has been interpreted as a consequence of the proper representation of spatial image information of land cover map into the MLE and LRE techniques. User's accuracy also reflects this new improvement in classification accuracy. As for "pasture", the classification using Landsat ETM+ and land cover map (Landsat TM) improved by 35.4% at LRE and 20.64% at MLE techniques. That class categories had similar spectral reflectance to other categories due to seasonal factors, though classification accuracy improved greatly when updated with the land cover map using GIS thematic map. The producer's accuracy of classification improved for most of the class categories. Especially, LRE technique producer's accuracy in "urban" and "farmland" improved by 25.7% and 18.7%, respectively. We obtained an improved classification accuracy for "pasture" areas, mainly because of the improvement of the "farmland" category. This causes of local changes of "pasture" into "urban area" or "farmland". This shows that accomplishing land cover classification using the existing GIS thematic map data could enable the extraction of the area with changes in land cover.

As a result, the expected improvements in the classification accuracy due to inclusion of GIS thematic data from additional sensors depend on the general discrimination ability of the multi-spectral data. Even by updating multi-spectral images containing relatively low discrimination information, and using partly inaccurate GIS thematic data, the combination resulted in significant improvements in the classification accuracy. Further research concerning this model will include evaluating it on different data sets. The performance of the model on combination data from other satellite sensors and on a larger test data set needs to be investigated. The general combination model can be adapted to other application areas, and the method should be further evaluated on a larger data set. Land cover maps, produced through the synthesis of various GIS spatial data and multi-spectral images, will be proved to be useful complimentary data in making more accurate decisions.

Acknowledgments

This work has been supported by National Research Laboratory grant from KISTEP(#m 10203000000702j000000510). The author would like to thank Prof. Choi Young-Eun and Dr. Park No-Wook at the KIGAM for valuable comments. We also wish to thank anonymous reviewers for valuable comments.

References

Benediktsson, J. A. and Sveinsson, J. R., 1997, Feature extraction for multisource data classification with artificial neural networks, *International Journal of Remote Sensing*, 18(4), 727-740.

Binaghi, E., Madella, P., Montesano, M. G., and Rampini, A., 1997, Fuzzy contextual classification of multisource remote sensing images, *IEEE Transactions on Geoscience and Remote Sensing*, 35, 326-340.

Chung, C. F., 1978, Computer program for the logistic model to estimate the probability of occurrence of discrete events, *Geological Society of Canada Paper*, 78-11.

Chung, C. F., Fabbri, A. G. and van Westen, C. J., 1995, Multivariate regression analysis for landslide hazard zonation, *Geographical Information Systems in Assessing Natural Hazards*, 107-133.

Clerici, A., Perego, S., Tellini, C. and Vescovi, P., 2002, A procedure for landslide susceptibility zonation by the conditional analysis method, *Geomorphology*, 48, 349-364.

Cox, D. R., 1969, *The Analysis of Binary Data*, Barnes & Nobel, INC.

Dai, A. and Khorram, S., 1999, Data fusion using artificial neural networks: a case study on multitemporal change analysis, *Computer, Environment and Urban Systems*, 23, 19-31.

Franklin, S. E., Peddle, D. R., Dechka, J. A. and Stenhouse, G. B., 2002, Evidential reasoning with Landsat TM, DEM and GIS data for land cover classification in support of grizzly bear habitat mapping, *International Journal of Remote Sensing*, 23(21), 4633-4652.

Guan, L., Anderson, A. and Sutton, J. P., 1997, A network of networks processing model for image regularization, *IEEE Transactions, Neural Networks*, 8, 169-174.

Hubert-Moy, L., Cotonnec, A., Le Du, L., Chardin, A. and Perez, P., 2001, A comparison of parametric classification procedures of remotely sensed data applied on different landscape units, *Remote Sensing of Environment*, 75, 174-187.

Johnson, N. L. and Kotz, S., 1972, *Distributions in Statistics: Continuous Multivariate Distribution*, 4, John Wiley & Sons, Yew York.

Lee, T., Richards, J. A. and Swain, P. H., 1987, Probabilistic and evidential approaches for multisource data analysis, *IEEE Transactions on Geoscience and Remote Sensing*, 25, 283-293.

Maselli, F., Conese, C., Filippis, T. and Romani, M., 1995, Integration of ancillary data into a maximum-likelihood classifier with nonparametric priors, *ISPRS Journal of Photogrammetric and Remote Sensing*, 50(2), 2-11.

Maxwell, E. L., 1976, Multivariate system analysis of multispectral imagery, *Photogrammetric Engineering and Remote Sensing*, 42, 1173-1186.

McLallen, G. J., 1990, *Discriminant Analysis and Statistical Pattern Recognition*, John Wiley & Sons, INC.

Peddle, D. R., 1995, MERCURY: an evidential reasoning image classifier, *Computers & Geosciences*, 21(10), 1163-1176.

Peddle, D. R. and Ferguson, D.T., 2002, Optimisation of multisource data analysis: an example using evidential reasoning for GIS data classification, *Computers and Geoscience*, 28, 45-52.

Press, S. J., 1972, *Applied Multivariate Analysis*, Holt, Rinehart and Winston, INC., New York.

Richards, J. A., 1995, *Remote Sensing Digital Image Analysis*, An Introduction, Springer-Verlag, New York.

Serpico, S. B., Bruzzone, L. and Roli, F., 1996, An experimental comparison of neural and statistical non-parametric algorithms for supervised classification of remote-sensing images, *Pattern Recognition Letters*, 17, 1331-1341.

Solaiman, B., Pierce, L. E. and Ulaby, F. T., 1999, Multisensor data fusion using fuzzy concepts: application to land-cover classification using ERS-1/JERS-1 SAR composites, *IEEE Transactions on Geoscience and Remote Sensing*, 37, 1316-1326.

Solberg, A. H., Jain, A. K. and Taxt, T., 1994, Multisource classification of remotely sensed data: fusion of Landsat TM and SAR images, *IEEE Transactions on Geoscience and Remote Sensing*, 32(4), 768-778.

Solberg, A. H., Taxt, T. and Jain, A. K., 1996, A

Markov random field model for classification of multisource satellite imagery, *IEEE Transactions on Geoscience and Remote Sensing*, 34(1), 100-113.

Solberg, A.H., 1999, Contextual data fusion applied to forest map revision, *IEEE Transactions on Geoscience and Remote Sensing*, 37(3), 1234-1243.

Tso, B. C. K. and Mather, P. M. 1999, Classification of multisource remote sensing imagery using a genetic algorithm and Markov random fields, *IEEE Transactions on Geoscience and Remote Sensing*, 37, 1255-1260.

Warrender, C. and Augusteijn, M., 1999, Fusion of image classifications using Bayesian techniques with Markov random fields, *International Journal of Remote Sensing*, 20(10), 1987-2002.

Received August 3, 2004
Accepted December 15, 2004

Correspondence : Dong-Ho Jang, National Research Laboratory (Harmful Algal Blooming Control), Kongju National University, gisrs@kongju.ac.kr, phone: 041-850-8558, fax: 041-850-8240)

교 신 : 장동호, 314-741 충남 공주시 신관동 182번지 공주대학교 지리학과(이메일 : gisrs@kongju.ac.kr 전화: 041-850-8558 팩스: 041-850-8240)